LANGMUIR Article
Cite This: Langmuir 2019, 35, 3568−3575
pubs.acs.org/Langmuir

Characterizing the Membrane-Disruptive Behavior of Dodecylglycerol Using Supported Lipid Bilayers

Bo Kyeong Yoon,[†] Joshua A. Jackman,[‡] Soohyun Park,[†] Natalia Mokrzecka,[†] and Nam-Joon Cho*[,†,§]

[†]School of Materials Science and Engineering, Nanyang Technological University, 50 Nanyang Avenue, 639798 Singapore
[‡]School of Chemical Engineering, Sungkyunkwan University, Suwon 16419, Republic of Korea
[§]School of Chemical and Biomedical Engineering, Nanyang Technological University, 62 Nanyang Drive, 637459 Singapore

ABSTRACT: Monoglycerides are esterified adducts of fatty acid and glycerol molecules that disrupt phospholipid membranes, leading to a wide range of biological functions such as antimicrobial activity. Among monoglycerides, glycerol monolaurate (GML) exhibits particularly high antimicrobial activity, although enzymatic hydrolysis of its ester group can diminish potency. Consequently, there have been efforts to identify more chemically stable versions of GML, most notably its alkylglycerol ether equivalent called dodecylglycerol (DDG). However, despite high structural similarity, biological studies indicate that DDG and GML are not functionally equivalent and it has been speculated that the two compounds might have different interaction profiles with phospholipid membranes. To address this outstanding question, herein, we employed supported lipid bilayer (SLB) platforms to experimentally characterize the interactions of DDG with phospholipid membranes. Quartz crystal microbalance-dissipation experiments identified that DDG causes concentration-dependent membrane morphological changes in SLBs and the overall extent of membrane remodeling events was greater than that caused by GML. In addition, time-lapsed fluorescence microscopy imaging experiments revealed that DDG causes extensive membrane tubulation that is distinct from how GML induces membrane budding. We discuss how differences in the head group properties of DDG and GML contribute to distinct membrane interaction profiles, offering insight into how the molecular design of DDG not only improves chemical stability but also enhances membrane-disruptive activity.

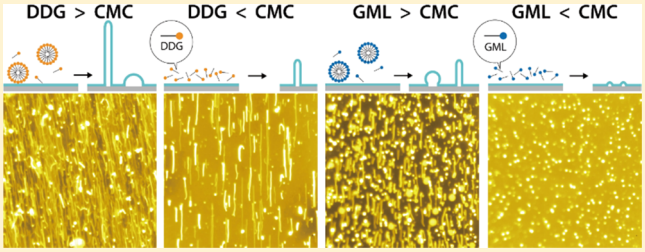

INTRODUCTION

Monoglycerides and other types of single-chain lipid amphiphiles can exhibit inhibitory activity against phospholipid membrane-enclosed pathogens, including enveloped viruses and bacteria, as well as display other types of biological functions.[1−4] Naturally found as a part of the innate immune system, these antimicrobial lipids work principally by physically disrupting cellular membranes and kill pathogens or inhibit growth depending on the lipid concentration.[5,6] Among them, glycerol monolaurate (GML) is one of the most potent antimicrobial lipids[7−9] and is the esterified adduct of lauric acid and glycerol. GML is widely used in food[10] and topical skin[11] products and is currently being evaluated as a promising pharmacological drug candidate.[12] However, the ester bond in GML is susceptible to hydrolysis by bacterial lipases, rendering GML sensitive to chemical degradation.[13,14] There have been efforts to design improved versions, including dodecylglycerol (DDG), which is the alkylglycerol ether equivalent of GML. With a nonhydrolyzable ether bond replacing the ester bond, DDG possesses greater chemical stability than GML and is hence a promising antimicrobial lipid.

Ved et al. first reported that DDG inhibits a wide range of bacteria more potently than GML.[15] The higher potency was attributed to enhanced chemical stability and greater retention in bacterial cells. Interestingly, DDG was found to inhibit bacterial growth by activating bacterial enzymes that break down the cell wall.[15] Later studies showed that DDG also inhibited metabolic processes associated with peptidoglycan synthesis[15,16] as well as lipid and lipoteichoic acid synthesis.[17] The wide range of metabolic activities affected by DDG treatment suggests that DDG disturbs bacterial cell membranes through a nonspecific mechanism, in turn, affecting the function of numerous, membrane-associated bacterial enzymes.[17] Although GML and DDG exhibit overlapping antibacterial activities, the aforementioned studies indicate that there are mechanistic distinctions between the two compounds. Such questions have spurred efforts to better understand the molecular self-assembly of DDG in the context of explaining its biological activity.

Biophysical experiments have demonstrated that the critical micelle concentration (CMC) of DDG is approximately 2-fold greater than its minimum inhibitory concentration for antibacterial activity, suggesting that DDG monomers might destabilize bacterial cell membranes.[18] This possibility was surprising because it is thought that antimicrobial lipids are principally active in the micellar state.[19] Additional reports

Received: January 25, 2019
Revised: February 4, 2019
Published: February 5, 2019

DOI: 10.1021/acs.langmuir.9b00244
Langmuir 2019, 35, 3568−3575

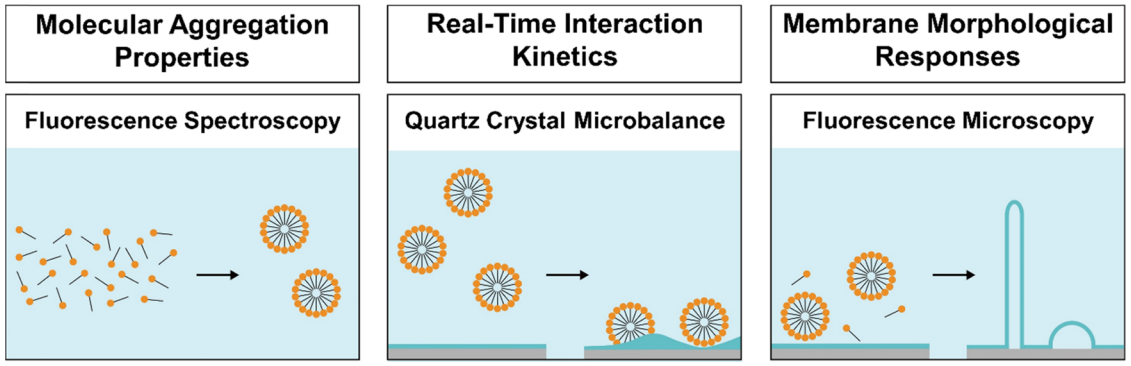

Figure 1. Overview of experimental strategy to characterize how DDG monomers and micelles interact with supported lipid bilayer platforms.

have corroborated that DDG affects membrane properties, including membrane fluidity.[20] It has also been shown that DDG can permeabilize *Staphylococcus aureus* cell membranes.[21] Together, the existing data support that the antimicrobial activity of DDG is related to the disruption of bacterial cell membranes although direct experimental characterization of the interactions between DDG and phospholipid membranes is lacking. Such findings motivate broader efforts to characterize how DDG interacts with phospholipid membranes. With continuing advances in lipid membrane-based nanoarchitectonic tools,[22,23] there is excellent opportunity to employ solid-supported model phospholipid membrane platforms that are compatible with a wide range of surface-sensitive measurement techniques for real-time interaction monitoring.[24,25]

Herein, we investigated the effects of DDG treatment on supported lipid bilayer (SLB) platforms and characterized real-time membrane morphological changes with the quartz crystal microbalance-dissipation (QCM-D) and time-lapsed fluorescence microscopy imaging techniques (Figure 1). A key advantage of this integrated experimental approach is that the interactions of antimicrobial lipids with a two-dimensional SLB cause extensive membrane remodeling, giving rise to three-dimensional membrane morphological responses that are compound specific and provide a discernible molecular interaction signature.[26,27] Comparative measurements were performed on structurally similar GML as it has been speculated that DDG and GML might affect the physical properties of phospholipid membranes to different extents.[28] Hence, GML provides a marker to evaluate the membrane-disruptive activity of DDG with respect to compound potency as well as the type and extent of membrane morphological changes. As such, our findings offer physicochemical insight into the interactions of DDG with phospholipid membranes and reveal that its high levels of biological activity are related to not only enhanced chemical stability but also greater membrane-disruptive activity.

EXPERIMENTAL SECTION

Materials. 1,2-Dioleoyl-*sn*-glycero-3-phosphocholine (DOPC) and 1,2-dioleoyl-*sn*-glycero-3-phosphoethanolamine-*N*-(lissamine rhodamine B sulfonyl) (ammonium salt) (Rh-PE) were obtained from Avanti Polar Lipids (Alabaster, AL). 1-*O*-Dodecyl-rac-glycerol (DDG) and glycerol monolaurate (GML) were obtained from Angene International (London, U.K.) and Abcam (Cambridge, U.K.), respectively. 1-Pyrenecarboxaldehyde was obtained from Sigma-Aldrich (St Louis, MO). Phosphate-buffered saline (PBS), Dulbecco's Modified Eagle Medium (DMEM), antibiotic−antimycotic, and trypsin were acquired from Gibco (Waltham, MA). Minimum Essential Medium (MEM) Alpha Modification and fetal bovine serum (FBS) were obtained from Hyclone (Logan, UT). Deionized water (>18 MΩ cm) was treated using a Milli-Q water purification system (MilliporeSigma, Burlington, MA) and was used for solution preparation.

Preparation of DDG and GML Solutions. Stock solutions (200 mM) of DDG and GML were prepared by dissolving lyophilized samples in the appropriate amount of absolute ethanol. Aliquots of the stock solution were then diluted 100-fold with PBS solution, and the final lipid concentration was 2 mM. For cell cytotoxicity experiments, the lyophilized samples were directly dissolved in the appropriate cell culture medium at a final concentration of 5 mM. In both cases, the lipid solutions were vortexed and then incubated at 60 °C for 30 min to increase solubility, followed by another round of extensive vortexing. After cooling, the lipid solutions were further diluted in 2-fold steps using either PBS or cell culture medium as appropriate depending on the experiment. All lipid solutions were prepared immediately before experiment.

Fluorescence Spectroscopy. The critical micelle concentration (CMC) values of DDG and GML were measured using a Cary Eclipse fluorescence spectrophotometer (Agilent, Santa Clara, CA), as previously described.[29] The fluorescence emission spectrum of the 1-pyrenecarboxaldehyde probe in PBS was measured in the absence and presence of varying concentrations of DDG or GML. The excitation wavelength was 365.5 nm, and the emission spectrum was scanned from 400 to 600 nm. All measurements were conducted at room temperature (~23 °C), and the maximum-intensity emission wavelength was recorded from each individual scan. A total of six scans were conducted per sample.

Quartz Crystal Microbalance-Dissipation (QCM-D). QCM-D experiments were conducted with a Q-Sense E4 instrument (Biolin Scientific AB, Stockholm, Sweden) to measure SLB perturbations, as reflected by changes in mass and viscoelastic properties of the adsorbed phospholipid film. The basic protocol steps are described in ref 27, and DOPC SLBs were fabricated using the solvent-assisted lipid bilayer (SALB) method.[30,31] The resonance frequency (Δf) and energy dissipation (ΔD) shifts of an SLB-coated, piezoelectric quartz crystal sensor chip were measured as a function of time.[32] The SLBs were formed on silica-coated sensor chips (model no. QSX 303, Biolin Scientific AB) that had a fundamental resonance frequency of 5 MHz. Before experiment, the sensor chips were washed with water and ethanol and then dried with nitrogen gas, followed by oxygen plasma treatment. All measurements were performed at 25.0 ± 0.5 °C, and all presented data were collected at the fifth overtone.

Time-Lapsed Fluorescence Microscopy Imaging. Epifluorescence microscopy experiments were conducted to directly observe membrane morphological responses in SLB platforms. An Eclipse TI-E inverted optical microscope with a 60× oil-immersion objective (NA 1.49) (Nikon, Tokyo, Japan) was used, and the micrographs were recorded with an iXon3-897 EMCCD camera (Andor Technology, Belfast, Northern Ireland). A mercury-fiber illuminator (Intenslight C-HGFIE, Nikon) was used to illuminate the fluorophores through a TRITC filter. The experiments were conducted within a flow-through, microfluidic chamber (sticky slide

DOI: 10.1021/acs.langmuir.9b00244
Langmuir 2019, 35, 3568−3575

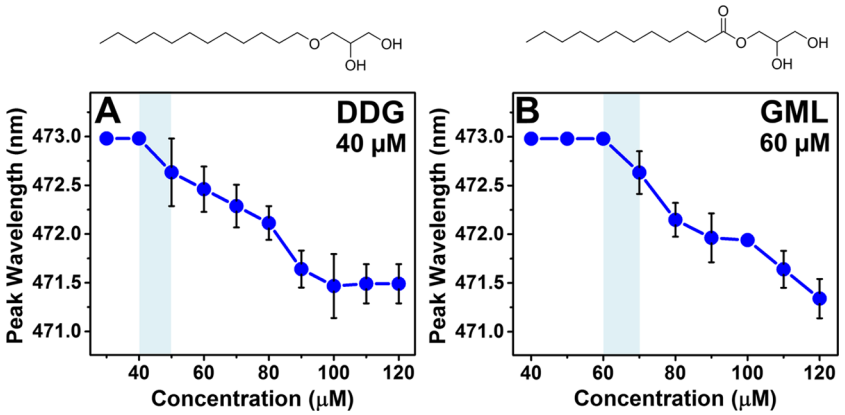

Figure 2. Critical micelle concentration values of DDG and GML determined by fluorescence spectroscopy. Maximum-intensity emission wavelength of 1-pyrenecarboxaldehyde is presented as a function of compound concentration in PBS solution for (A) DDG and (B) GML. The corresponding molecular structures of each compound are presented above each graph. Each data point is the average of six technical replicates (n = 6). The mean and standard deviation (expressed as the error bars) are presented for each data point. The CMC value is defined as the highest test concentration at which no peak shift occurs.

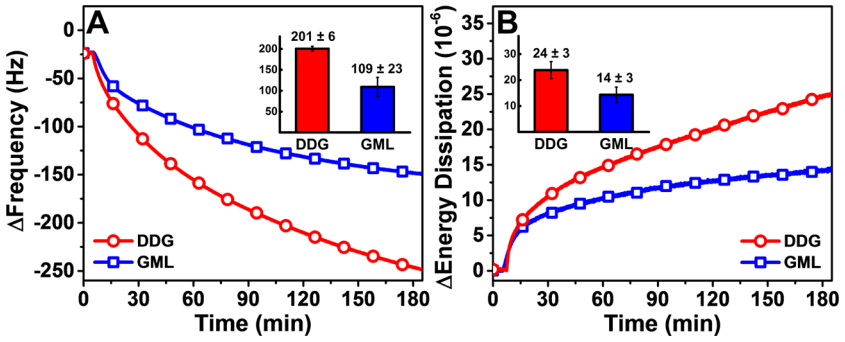

Figure 3. QCM-D measurements of SLB membrane morphological responses induced by DDG and GML micelles. Changes in (A) resonance frequency and (B) energy dissipation were monitored as a function of time upon DDG (red line with circles) or GML (blue line with squares) addition to preformed DOPC SLBs. The initial baseline values at t = 0 min correspond to the QCM-D measurement shifts due to SLB formation. The inset boxes show the magnitude of the QCM-D measurement responses, as indicated by the mean and standard deviation (n = 3). DDG or GML was added to the DOPC SLB at t = 5 min after the measurement signals stabilized.

VI 0.4, ibidi GmbH, Martinsried, Germany). DOPC SLBs (containing 0.5 mol % of fluorescently labeled Rh-PE lipid) were fabricated using the SALB method on glass surfaces. After SLB fabrication, the microfluidic chamber was extensively rinsed with PBS before DDG or GML was added at a flow rate of 50 μL/min, controlled by a peristaltic pump. Time-lapsed micrographs were recorded every 3 s for a total duration of 30 min under ambient room-temperature conditions (~23 °C).

Cell Viability Testing. The effects of DDG and GML on human cell lines were tested by measuring the level of dehydrogenase activity with the cell counting kit-8 (CCK-8) (Dojindo Molecular Technologies, Rockville, MD). Human lung fibroblast cells (MRC-5) (RIKEN BioResource Center, Tsukuba, Japan) were cultured in MEM Alpha Modification supplemented with 10% FBS and 1% streptomycin/amphotericin B/penicillin. Human keratinocyte cells (HaCaT) (CLS Cell Lines Service, Eppelheim, Germany) were cultured in DMEM containing 4.5 g/L D-glucose, L-glutamine, and 110 mg/L sodium pyruvate supplemented with 10% FBS and 1% antibiotic–antimycotic. Both cell lines were cultured at 37 °C in a 5% CO_2 environment. Harvested cells in the exponential growth phase were seeded into a 96-well tissue culture plate at a density of 5000 and 10 000 cells per well for MRC-5 and HaCaT cells, respectively, and incubated at 37 °C in a 5% CO_2 environment for 24 h. Afterward, a media-exchange step was performed and fresh media containing the appropriate concentration of DDG or GML (5000 to 10 μM in a 2-fold dilution series) was added. The cells were further incubated at 37 °C in a 5% CO_2 environment for an additional 24 h. Then, the treated cells were incubated in 10% CCK-8 solution containing water-soluble tetrazolium salt (WST-8), at 37 °C in a 5% CO_2 environment for 90 min. The generation of formazan dye as the result of WST-8 reduction caused by dehydrogenase activity was analyzed by measuring sample absorbance at 450 nm wavelength using a microplate reader (Infinite M200 Pro, Tecan, Zurich, Switzerland). Cells without treatment and cells treated with 1% Triton X-100 were used as the negative and positive controls, respectively. All experiments were conducted in triplicate.

RESULTS AND DISCUSSION

DDG Has a Lower CMC Value than GML. It has been suggested that single-chain antimicrobial lipids form micelles, which are the self-assembled structure that disrupts phospholipid membranes.[19] Therefore, we first measured the CMC values of DDG and GML in PBS by fluorescence spectroscopy experiments (Figure 2). This technique is a well-established method for CMC determination by detecting the change in emission properties of solution-phase fluorescent probe molecules when they partition into the hydrophobic interior of micelles.[29,33,34] Specifically, the maximum emission wavelength decreases due to a lower dielectric constant of the surrounding hydrophobic environment.[34] In blank PBS, the fluorescent probe (1-pyrenecarboxaldehyde) had a maximum-intensity emission wavelength of 473 nm and its emission properties remained constant in the presence of DDG

DOI: 10.1021/acs.langmuir.9b00244
Langmuir 2019, 35, 3568–3575

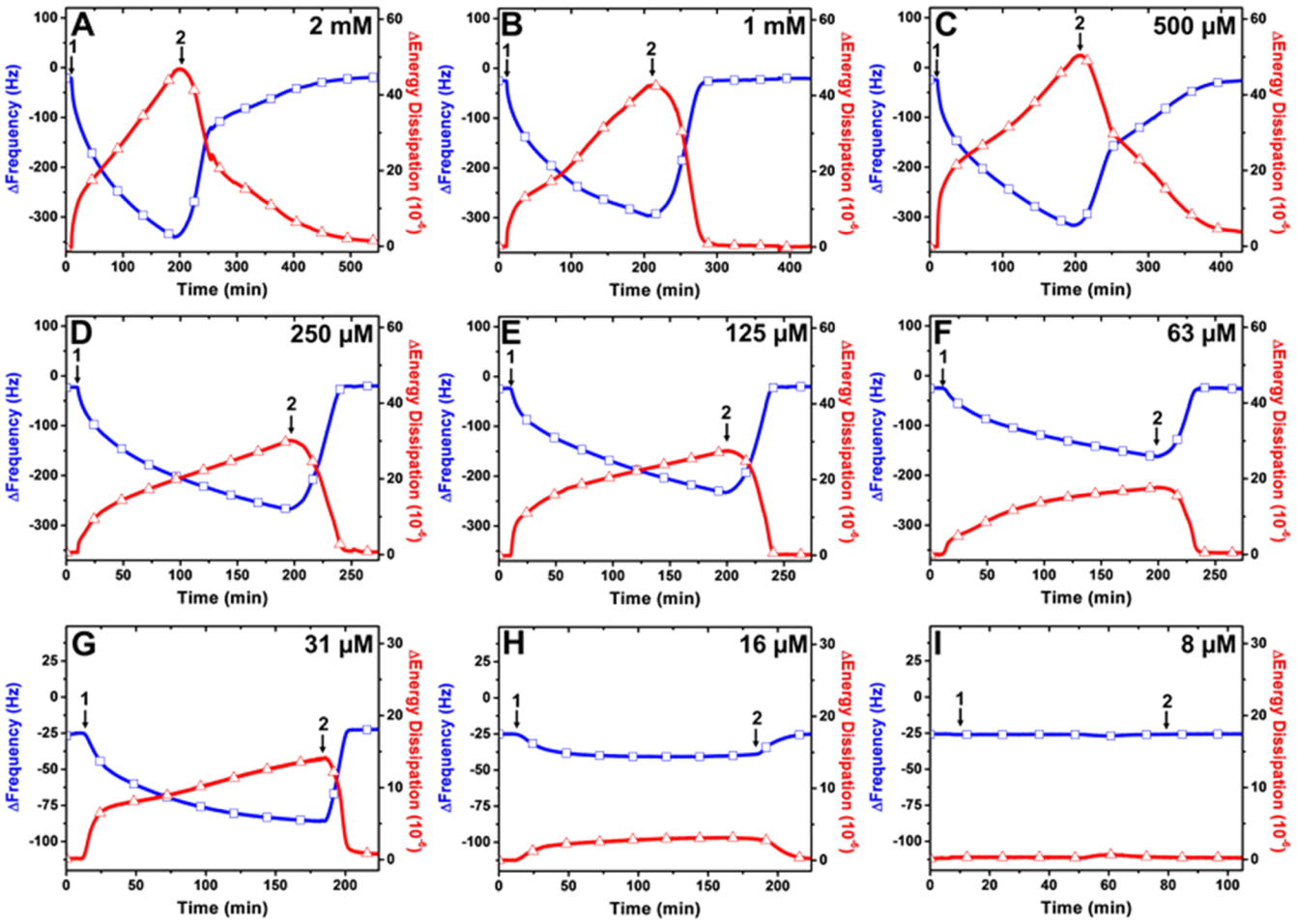

Figure 4. QCM-D investigation of concentration-dependent DDG treatment on SLB membrane morphological responses. Δf (blue line with squares) and ΔD (red line with triangles) shifts as a function of time are presented for DOPC SLBs upon addition of (A) 2 mM, (B) 1 mM, (C) 500 μM, (D) 250 μM, (E) 125 μM, (F) 63 μM, (G) 31 μM, (H) 16 μM, and (I) 8 μM DDG concentrations. The initial measurement values correspond to an SLB on a silica-coated sensor chip surface. DDG was added at t = 10 min (arrow 1), and a PBS washing step was performed (arrow 2).

monomers. Upon the onset of DDG micelle formation, the maximum-intensity emission wavelength decreased and the CMC of DDG was determined to be 40 μM, which agrees with literature values[18] (Figure 2A). In addition, the CMC of GML was determined to be 60 μM, which also agrees with literature values[35] (Figure 2B). Together, the results indicate the DDG has a lower CMC value than GML. This finding can be rationalized by the greater polarity of ester bonds in GML, as compared with ether bonds in DDG. Greater polarity increases the thermodynamic barrier for micelle formation to occur due to more repulsive dipole−dipole interactions,[36,37] hence supporting GML having a higher CMC value.

DDG Causes Larger Membrane Morphological Changes than GML. We then conducted QCM-D experiments to characterize the membrane-disruptive interactions of DDG and GML micelles against zwitterionic DOPC SLBs (Figure 3). The zwitterionic DOPC lipid composition was selected because it yields high-quality SLBs and phosphatidylcholine lipids are one of the most widely found lipids in biological membranes. Notably, DOPC SLBs have also proven useful for distinguishing various types of membrane morphological responses induced by antimicrobial lipids. When an antimicrobial lipid is added to the SLB, it can trigger three-dimensional membrane morphological changes in response to an applied membrane strain.[38] Depending on the type of antimicrobial lipid and environmental conditions, different types of morphological changes occur and real-time QCM-D measurements enable tracking of corresponding changes in the mass and viscoelastic properties of the SLB platform.[27,29,39,40] In the experiments, the DOPC SLBs were initially fabricated by using the SALB method and yielded complete SLBs, as indicated by final resonance frequency (Δf) and energy dissipation (ΔD) shifts of -26 ± 2 Hz and $0.3 \pm 0.2 \times 10^{-6}$, respectively.[24] Then, the subsequent addition of 125 μM DDG or GML to a DOPC SLB triggered large-scale membrane morphological changes, as further indicated by the Δf and ΔD shifts.[27] The response profiles were qualitatively similar for the two compounds, as might be expected considering that DDG and GML both exhibit a nonionic character. However, quantitatively, DDG treatment caused significantly larger measurement responses, which are indicative of more extensive morphological changes. The magnitudes of the net Δf shift were 201 ± 6 and 109 ± 23 Hz for DDG and GML treatments, respectively (Figure 3A). Likewise, the corresponding net ΔD shifts were $24 \pm 3 \times 10^{-6}$ and $14 \pm 3 \times 10^{-6}$ for DDG and GML treatments, respectively (Figure 3B). Taken together, the QCM-D measurement responses demonstrate that DDG

DOI: 10.1021/acs.langmuir.9b00244
Langmuir 2019, 35, 3568−3575

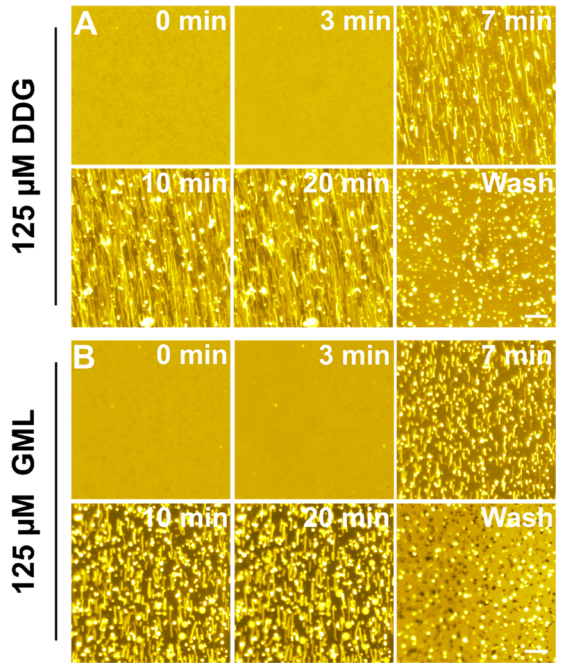

Figure 5. Time-lapsed fluorescence microscopy imaging of DDG and GML micelles, inducing membrane morphological responses in SLBs. Image snapshots at various time points after addition of (A) 125 μM DDG and (B) 125 μM GML to DOPC SLBs. t = 0 min corresponds to the introduction of DDG or GML into the measurement chamber. Scale bars are 20 μm.

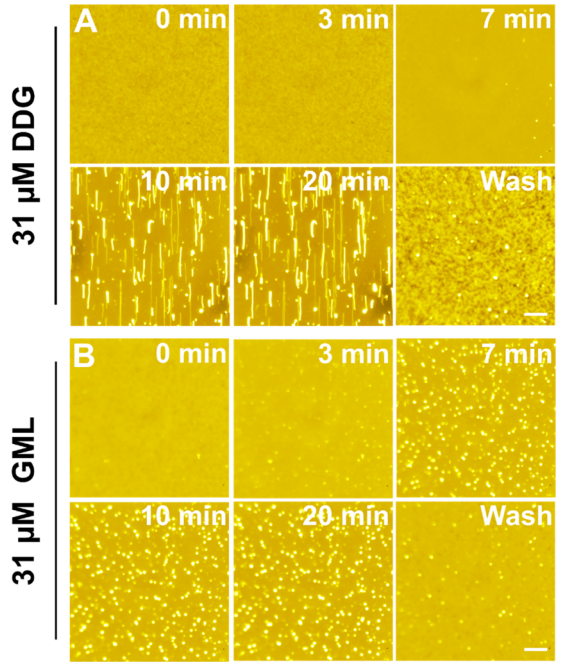

Figure 6. Time-lapsed fluorescence microscopy imaging of low-concentration DDG and GML inducing membrane morphological responses in SLBs. Image snapshots at various time points after addition of (A) 31 μM DDG and (B) 31 μM GML to DOPC SLBs. t = 0 min corresponds to the introduction of DDG or GML into the measurement chamber. Scale bars are 20 μm.

micelles cause more significant membrane morphological changes to SLBs than GML micelles.

DDG Exhibits Concentration-Dependent, Membrane-Disruptive Activity against SLBs. We conducted additional QCM-D experiments to investigate how the DDG concentration affects membrane-disruptive interactions with SLBs (Figure 4). Treatment with 500−2000 μM DDG caused large Δf (>250 Hz) and ΔD (>40 × 10^{-6}) shifts (Figure 4A−C). Within this range, the magnitude of the QCM-D responses was largely independent of the DDG concentration. Treatment with 31−250 μM DDG caused similar response profiles, but the magnitude of the QCM-D responses varied according to the DDG concentration (Figure 4D−G). Larger measurement responses occurred with greater DDG concentrations, supporting that the extent of DDG-induced changes in membrane morphology depends on the DDG concentration. On the other hand, treatment with 16 μM DDG led to smaller morphological changes and there were negligible changes upon treatment with 8 μM DDG (Figure 4H,I). Together, the data support that DDG exhibits concentration-dependent disruptive activity against SLBs and it is principally active in the micellar state. Nevertheless, it is noteworthy that DDG is also active against SLBs down to roughly one-half of its CMC value. This finding is consistent with past biological studies indicating that DDG inhibits *Enterococcus faecium* at concentrations down to one-half of its CMC value,[18] suggesting that membrane-disruptive activity of DDG is caused by not only DDG micelles but also DDG in a premicellar aggregation state as well.[41,42] In this respect, the concentration-dependent trend in DDG activity is similar to that of other monoglycerides like GML and the importance of molecular aggregation state on membrane-disruptive behavior has also been reported for additional types of membrane-intercalating agents with hydrophobic moieties such as ionic liquids.[43,44]

DDG Micelles Cause Tubule Formation and Entanglement. To further investigate the membrane morphological changes in SLBs, we conducted time-lapsed fluorescence microscopy imaging experiments (Figure 5). DDG (125 μM) was added to a fluorescently labeled SLB and three-dimensional membrane remodeling events were observed in response to the applied strain within the SLB (Figure 5A). Within 7 min, a large number of long tubular protrusions emerged from the SLB and were oriented in the flow direction. Over time, some of the tubules became entangled, coalescing and forming small spherical buds. The coexistence of a large number of elongated tubules and a few buds remained stable up to 20 min when a washing step was performed, replacing the continuously flowing DDG solution with pure aqueous buffer. Upon buffer washing, most of the elongated tubules were removed whereas bright spots, likely the nucleation sites from which the tubules emerged, became apparent near the SLB surface. In marked contrast, 125 μM GML caused the formation of appreciably smaller tubules that quickly became entangled and formed a much higher fraction of spherical buds (Figure 5B). Under the flow condition, the entangled tubules and spherical buds remained stable until a buffer washing step was performed, resulting in the appearance of porelike defects within the SLB. Altogether, the data indicate that DDG principally causes formation of elongated tubules whereas GML induces the formation of much shorter, entangled tubules leading to spherical budding. Consistent with the QCM-D data, these findings support that DDG and GML exhibit distinct membrane interaction profiles on account of inducing different membrane strain profiles.

DOI: 10.1021/acs.langmuir.9b00244
Langmuir 2019, 35, 3568−3575

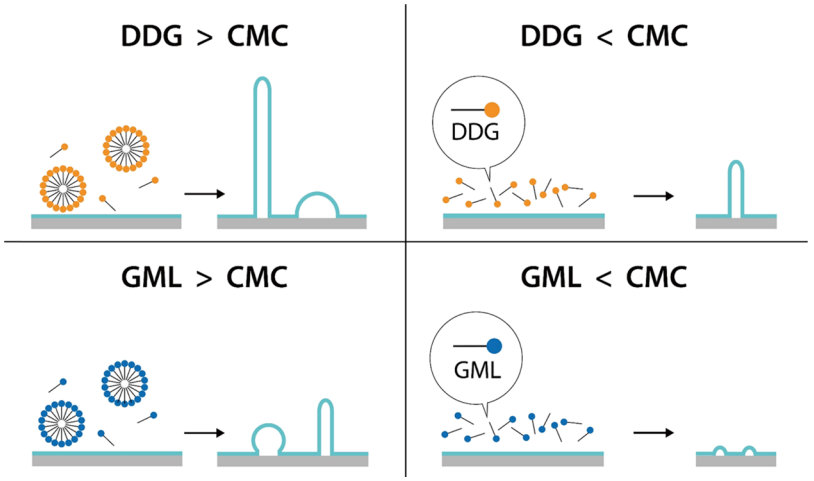

Figure 7. Schematic illustrations depicting the types of membrane morphological changes that occur in SLB platforms due to DDG and GML interactions. The drawings are based on the fluorescence microscopy results and describe the membrane-disruptive effects of both compounds above and below their corresponding CMC values, respectively.

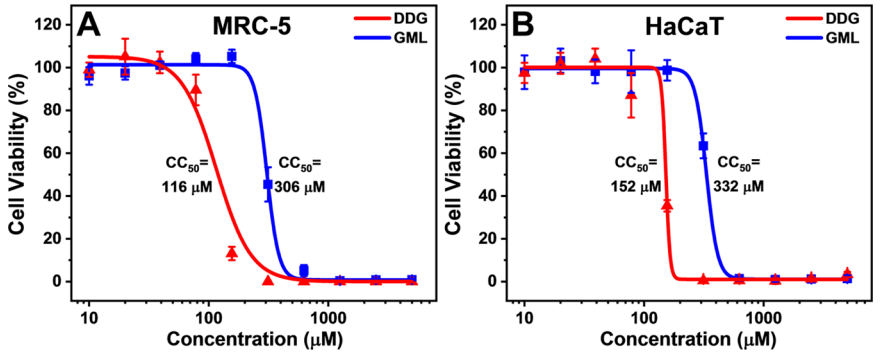

Figure 8. Concentration-dependent effects of DDG and GML on human cell viability. Cell viability percentages for (A) MRC-5 lung fibroblast cells and (B) HaCaT skin keratinocyte cells are presented as a function of DDG (red line with triangles) or GML (blue line with squares) concentration. Experiments were conducted in triplicate and data are reported as the mean and standard deviation.

Low-Concentration DDG Causes Membrane Disruption. Using time-lapsed fluorescence microscopy imaging, we also investigated the effect of adding 31 μM DDG to DOPC SLBs (Figure 6). In this concentration range, DDG is likely present as a mixture of monomers and premicellar aggregates and exhibits membrane-disruptive activity, as indicated by the aforementioned QCM-D data. Upon DDG addition, it was observed that elongated tubules began to protrude from the SLB within 10 min (Figure 6A). After a buffer washing step was performed, the tubules were washed away whereas a large number of porelike defects within the SLB became apparent. By contrast, 31 μM GML induced small membrane protrusions to evolve from the SLB without consequent membrane disruption (Figure 6B). Most of the protrusions disappeared upon a buffer washing step, resulting in the appearance of a relatively uniform SLB. Taken together, the data support that DDG exhibits more potent membrane-disruptive activity against SLBs than GML, including evidence of membrane disruption at DDG concentrations indicative of the presence of premicellar aggregates. An illustrative summary of the types of membrane morphological responses that are caused by DDG and GML above and below CMC is presented in Figure 7.

DDG Is More Cytotoxic against Human Cells than GML. To corroborate the biophysical findings, we also tested the concentration-dependent effects of DDG and GML in cell culture medium on the viability of two representative human cell lines: lung fibroblasts (MRC-5) and skin keratinocytes (HaCaT) (Figure 8). The level of dehydrogenase activity, an important marker of cellular metabolism, was measured as an indicator of the overall cell viability. For MRC-5 cells, there was a marked difference in the cytotoxicity levels of the two compounds and the corresponding 50% cell cytotoxicity (CC_{50}) values were 116 and 306 μM for DDG and GML, respectively (Figure 8A). Similar inhibitory effects were observed with HaCaT cells, and the CC_{50} values were 152 and 332 μM for DDG and GML, respectively (Figure 8B). These data support that DDG exhibits more potent cytotoxicity than GML,[28,45] a finding that is aligned with our key observation that DDG exhibits greater membrane-disruptive activity than GML. Given these biological implications, such findings also motivate future work to better understand how antimicrobial lipids such as DDG target membranes with complex lipid compositions, including raft-containing ones.[46]

CONCLUSIONS

The emerging application potential of antimicrobial lipids is aided by efforts to understand how they interact with phospholipid membranes, which is the presumed target within pathogens such as bacteria and enveloped viruses. Toward this goal, we have developed SLB platforms to study the mechanism of action of antimicrobial lipids, complementing

DOI: 10.1021/acs.langmuir.9b00244
Langmuir 2019, 35, 3568−3575

biological studies while gaining fundamental insight into key physicochemical parameters. Within this scope, in the present work, we have focused on studying DDG, which is the alkylglycerol ether equivalent of the GML monoglyceride. It has long been presumed that DDG exhibits greater biological activity than GML due to enhanced chemical stability; however, membrane interaction studies were lacking. Using SLB platforms, we identified that DDG exhibits greater membrane-disruptive activity than GML on account of higher potency, more pronounced membrane morphological changes, and a distinct membrane interaction profile. These findings indicate that the molecular design of DDG not only improves chemical stability but also increases membrane-disruptive activity. Although most antimicrobial lipids are naturally found, understanding how changes in molecular structure, as evidenced by the case of DDG and GML, can lead to multifaceted effects on chemical and biophysical properties might provide a framework to rationally engineer antimicrobial lipids with advantageous features.

AUTHOR INFORMATION

Corresponding Author

*E-mail: njcho@ntu.edu.sg.

ORCID

Joshua A. Jackman: 0000-0002-1800-8102

Nam-Joon Cho: 0000-0002-8692-8955

Notes

The authors declare no competing financial interest.

ACKNOWLEDGMENTS

This work was supported by a National Research Foundation Proof-of-Concept Grant (NRF2015NRF-POC001-019), an A*STAR-NTU-NHG Skin Research Grant (SRG/14028), and the Creative Materials Discovery Program through the National Research Foundation of Korea (NRF) that is funded by the Ministry of Science, ICT, and Future Planning (2016M3D1A1024098).

REFERENCES

(1) Thormar, H.; Hilmarsson, H. The Role of Microbicidal Lipids in Host Defense against Pathogens and Their Potential as Therapeutic Agents. *Chem. Phys. Lipids* **2007**, *150*, 1−11.

(2) Jackman, J. A.; Yoon, B. K.; Li, D.; Cho, N.-J. Nanotechnology Formulations for Antibacterial Free Fatty Acids and Monoglycerides. *Molecules* **2016**, *21*, No. 305.

(3) Yoon, B.; Jackman, J.; Valle-González, E.; Cho, N.-J. Antibacterial Free Fatty Acids and Monoglycerides: Biological Activities, Experimental Testing, and Therapeutic Applications. *Int. J. Mol. Sci.* **2018**, *19*, No. 1114.

(4) Desbois, A. P. Potential Applications of Antimicrobial Fatty Acids in Medicine, Agriculture and Other Industries. *Recent Pat. Anti-Infect. Drug Discovery* **2012**, *7*, 111−122.

(5) Drake, D. R.; Brogden, K. A.; Dawson, D. V.; Wertz, P. W. Thematic Review Series: Skin Lipids. Antimicrobial Lipids at the Skin Surface. *J. Lipid Res.* **2008**, *49*, 4−11.

(6) Desbois, A. P.; Smith, V. J. Antibacterial Free Fatty Acids: Activities, Mechanisms of Action and Biotechnological Potential. *Appl. Microbiol. Biotechnol.* **2010**, *85*, 1629−1642.

(7) Kabara, J. J.; Swieczkowski, D. M.; Conley, A. J.; Truant, J. P. Fatty Acids and Derivatives as Antimicrobial Agents. *Antimicrob. Agents Chemother.* **1972**, *2*, 23−28.

(8) Kabara, J. J.; Vrable, R.; Lie Ken Jie, M. Antimicrobial Lipids: Natural and Synthetic Fatty Acids and Monoglycerides. *Lipids* **1977**, *12*, 753−759.

(9) Kabara, J. J. Antimicrobial Agents Derived from Fatty Acids. *J. Am. Oil Chem. Soc.* **1984**, *61*, 397−403.

(10) Kabara, J. J. A New Preservative System for Food. *J. Food Saf.* **1982**, *4*, 13−25.

(11) Carpo, B. G.; Verallo-Rowell, V. M.; Kabara, J. Novel Antibacterial Activity of Monolaurin Compared with Conventional Antibiotics against Organisms from Skin Infections: an In Vitro Study. *J. Drugs Dermatol.* **2007**, *6*, 991−998.

(12) Li, Q.; Estes, J. D.; Schlievert, P. M.; Duan, L.; Brosnahan, A. J.; Southern, P. J.; Reilly, C. S.; Peterson, M. L.; Schultz-Darken, N.; Brunner, K. G.; et al. Glycerol Monolaurate Prevents Mucosal SIV Transmission. *Nature* **2009**, *458*, No. 1034.

(13) Ruzin, A.; Novick, R. P. Equivalence of Lauric Acid and Glycerol Monolaurate as Inhibitors of Signal Transduction in *Staphylococcus aureus*. *J. Bacteriol.* **2000**, *182*, 2668−2671.

(14) Schlievert, P.; Deringer, J. R.; Kim, M. H.; Projan, S. J.; Novick, R. Effect of Glycerol Monolaurate on Bacterial Growth and Toxin Production. *Antimicrob. Agents Chemother.* **1992**, *36*, 626−631.

(15) Ved, H.; Gustow, E.; Mahadevan, V.; Pieringer, R. Dodecylglycerol. A New Type of Antibacterial Agent which Stimulates Autolysin Activity in *Streptococcus faecium* ATCC 9790. *J. Biol. Chem.* **1984**, *259*, 8115−8121.

(16) Ved, H.; Gustow, E.; Pieringer, R. A. The Involvement of the Proteinase of *Streptococcus faecium* ATCC 9790 in the Stimulation of its Autolysin Activity by Dodecylglycerol. *J. Biol. Chem.* **1984**, *259*, 8122−8124.

(17) Brissette, J. L.; Cabacungan, E. A.; Pieringer, R. A. Studies on the Antibacterial Activity of Dodecylglycerol. Its Limited Metabolism and Inhibition of Glycerolipid and Lipoteichoic Acid Biosynthesis in *Streptococcus* mutans BHT. *J. Biol. Chem.* **1986**, *261*, 6338−6345.

(18) Ved, H.; Gustow, E.; Pieringer, R. A. Synergism between Penicillin G and the Antimicrobial Ether Lipid, rac-1-dodecylglycerol, Acting Below its Critical Micelle Concentration. *Lipids* **1990**, *25*, 119−121.

(19) Sun, C. Q.; O'Connor, C. J.; Roberton, A. M. Antibacterial Actions of Fatty Acids and Monoglycerides against *Helicobacter pylori*. *FEMS Immunol. Med. Microbiol.* **2003**, *36*, 9−17.

(20) Haynes, M.; Buckley, H. R.; Higgins, M. L.; Pieringer, R. A. Synergism between the Antifungal Agents Amphotericin B and Alkyl Glycerol Ethers. *Antimicrob. Agents Chemother.* **1994**, *38*, 1523−1529.

(21) Parsons, J. B.; Yao, J.; Frank, M. W.; Jackson, P.; Rock, C. O. Membrane Disruption by Antimicrobial Fatty Acids Releases Low Molecular Weight Proteins from *Staphylococcus aureus*. *J. Bacteriol.* **2012**, *194*, 5294−5304.

(22) Komiyama, M.; Yoshimoto, K.; Sisido, M.; Ariga, K. Chemistry Can Make Strict and Fuzzy Controls for Bio-Systems: DNA Nanoarchitectonics and Cell-Macromolecular Nanoarchitectonics. *Bull. Chem. Soc. Jpn.* **2017**, *90*, 967−1004.

(23) Thanuja, M.; Anupama, C.; Ranganath, S. H. Bioengineered Cellular and Cell Membrane-Derived Vehicles for Actively Targeted Drug Delivery: So Near and Yet So Far. *Adv. Drug Delivery Rev.* **2018**, *132*, 57−80.

(24) Cho, N.-J.; Frank, C. W.; Kasemo, B.; Höök, F. Quartz Crystal Microbalance with Dissipation Monitoring of Supported Lipid Bilayers on Various Substrates. *Nat. Protoc.* **2010**, *5*, No. 1096.

(25) Mashaghi, A.; Mashaghi, S.; Reviakine, I.; Heeren, R. M.; Sandoghdar, V.; Bonn, M. Label-Free Characterization of Biomembranes: from Structure to Dynamics. *Chem. Soc. Rev.* **2014**, *43*, 887−900.

(26) Thid, D.; Benkoski, J. J.; Svedhem, S.; Kasemo, B.; Gold, J. DHA-Induced Changes of Supported Lipid Membrane Morphology. *Langmuir* **2007**, *23*, 5878−5881.

(27) Yoon, B. K.; Jackman, J. A.; Kim, M. C.; Cho, N.-J. Spectrum of Membrane Morphological Responses to Antibacterial Fatty Acids and Related Surfactants. *Langmuir* **2015**, *31*, 10223−10232.

(28) Lin, Y.-C.; Schlievert, P. M.; Anderson, M. J.; Fair, C. L.; Schaefers, M. M.; Muthyala, R.; Peterson, M. L. Glycerol Monolaurate and Dodecylglycerol Effects on *Staphylococcus aureus* and Toxic Shock

DOI: 10.1021/acs.langmuir.9b00244
Langmuir 2019, 35, 3568−3575

Syndrome Toxin-1 In Vitro and In Vivo. *PLoS One* **2009**, *4*, No. e7499.
(29) Yoon, B. K.; Jackman, J. A.; Kim, M. C.; Sut, T. N.; Cho, N.-J. Correlating Membrane Morphological Responses with Micellar Aggregation Behavior of Capric Acid and Monocaprin. *Langmuir* **2017**, *33*, 2750−2759.
(30) Tabaei, S. R.; Choi, J.-H.; Haw Zan, G.; Zhdanov, V. P.; Cho, N.-J. Solvent-Assisted Lipid Bilayer Formation on Silicon Dioxide and Gold. *Langmuir* **2014**, *30*, 10363−10373.
(31) Tabaei, S. R.; Jackman, J. A.; Kim, S.-O.; Zhdanov, V. P.; Cho, N.-J. Solvent-Assisted Lipid Self-Assembly at Hydrophilic Surfaces: Factors Influencing the Formation of Supported Membranes. *Langmuir* **2015**, *31*, 3125−3134.
(32) Rodahl, M.; Höök, F.; Krozer, A.; Brzezinski, P.; Kasemo, B. Quartz Crystal Microbalance Setup for Frequency and Q-factor Measurements in Gaseous and Liquid Environments. *Rev. Sci. Instrum.* **1995**, *66*, 3924−3930.
(33) Domínguez, A.; Fernández, A.; González, N.; Iglesias, E.; Montenegro, L. Determination of Critical Micelle Concentration of Some Surfactants by Three Techniques. *J. Chem. Educ.* **1997**, *74*, No. 1227.
(34) Goddard, E.; Turro, N.; Kuo, P.; Ananthapadmanabhan, K. Fluorescence Probes for Critical Micelle Concentration Determination. *Langmuir* **1985**, *1*, 352−355.
(35) Inácio, Â. S.; Mesquita, K. A.; Baptista, M.; Ramalho-Santos, J.; Vaz, W. L.; Vieira, O. V. In Vitro Surfactant Structure-Toxicity Relationships: Implications for Surfactant Use in Sexually Transmitted Infection Prophylaxis and Contraception. *PLoS One* **2011**, *6*, No. e19850.
(36) Nagarajan, R.; Ruckenstein, E. Aggregation of Amphiphiles as Micelles or Vesicles in Aqueous Media. *J. Colloid Interface Sci.* **1979**, *71*, 580−604.
(37) Nagarajan, R.; Ruckenstein, E. Theory of Surfactant Self-Assembly: a Predictive Molecular Thermodynamic Approach. *Langmuir* **1991**, *7*, 2934−2969.
(38) Staykova, M.; Arroyo, M.; Rahimi, M.; Stone, H. A. Confined Bilayers Passively Regulate Shape and Stress. *Phys. Rev. Lett.* **2013**, *110*, No. 028101.
(39) Kawakami, L. M.; Yoon, B. K.; Jackman, J. A.; Knoll, W.; Weiss, P. S.; Cho, N.-J. Understanding How Sterols Regulate Membrane Remodeling in Supported Lipid Bilayers. *Langmuir* **2017**, *33*, 14756−14765.
(40) Valle-González, E. R.; Jackman, J. A.; Yoon, B. K.; Park, S.; Sut, T. N.; Cho, N.-J. Characterizing How Acidic pH Conditions Affect the Membrane-Disruptive Activities of Lauric Acid and Glycerol Monolaurate. *Langmuir* **2018**, *34*, 13745−13753.
(41) Hadgiivanova, R.; Diamant, H. Premicellar Aggregation of Amphiphilic Molecules. *J. Phys. Chem. B* **2007**, *111*, 8854−8859.
(42) LeBard, D. N.; Levine, B. G.; DeVane, R.; Shinoda, W.; Klein, M. L. Premicelles and Monomer Exchange in Aqueous Surfactant Solutions Above and Below the Critical Micelle Concentration. *Chem. Phys. Lett.* **2012**, *522*, 38−42.
(43) Losada-Pérez, P.; Khorshid, M.; Renner, F. U. Interactions of Aqueous Imidazolium-Based Ionic Liquid Mixtures with Solid-Supported Phospholipid Vesicles. *PLoS One* **2016**, *11*, No. e0163518.
(44) Witos, J.; Russo, G.; Ruokonen, S.-K.; Wiedmer, S. K. Unraveling Interactions between Ionic Liquids and Phospholipid Vesicles Using Nanoplasmonic Sensing. *Langmuir* **2017**, *33*, 1066−1076.
(45) Poulsen, C.; Mehalick, L. A.; Fischer, C. L.; Lanzel, E. A.; Bates, A. M.; Walters, K. S.; Cavanaugh, J. E.; Guthmiller, J. M.; Johnson, G. K.; Wertz, P. W. Differential Cytotoxicity of Long-Chain Bases for Human Oral Gingival Epithelial Keratinocytes, Oral Fibroblasts, and Dendritic Cells. *Toxicol. Lett.* **2015**, *237*, 21−29.
(46) Losada-Pérez, P.; Khorshid, M.; Hermans, C.; Robijns, T.; Peeters, M.; Jiménez-Monroy, K.; Truong, L.; Wagner, P. Melittin Disruption of Raft and Non-Raft-Forming Biomimetic Membranes: A Study by Quartz Crystal Microbalance with Dissipation Monitoring. *Colloids Surf., B* **2014**, *123*, 938−944.

DOI: 10.1021/acs.langmuir.9b00244
Langmuir 2019, 35, 3568−3575